Dynamic Imaging of Transient Metabolic Processes by Small-Animal PET for the Evaluation of Photosensitizers in Photodynamic Therapy of Cancer

Véronique Bérard, Jacques A. Rousseau, Jules Cadorette, Laurent Hubert, M'hamed Bentourkia, Johan E. van Lier, and Roger Lecomte

Sherbrooke Molecular Imaging Centre, Étienne-LeBel Clinical Research Centre, Centre Hospitalier Universitaire de Sherbrooke, Sherbrooke, Quebec, Canada; and Department of Nuclear Medicine and Radiobiology, Faculty of Medicine and Health Sciences, Université de Sherbrooke, Sherbrooke, Quebec, Canada

This study evaluated the potential use of dynamic PET to monitor transient metabolic processes and to investigate the mechanisms of action of new photosensitizing drugs in the photodynamic therapy (PDT) of cancer. **Methods:** Rats bearing 2 mammary tumors received different phthalocyanine-based photosensitizers. The following day, the animals were positioned in a Sherbrooke small-animal PET scanner and continuously infused with ^{18}F-FDG while dynamic images were acquired for 2 h. During that period, one of the 2 tumors was exposed for 30 min to red light delivered by a small diode laser to activate PDT. **Results:** ^{18}F-FDG time–activity curves during PDT showed distinct transient patterns characterized by a drop and subsequent recovery of tumor ^{18}F-FDG uptake rates. Variations in these rates and response delay parameters revealed tumoral and systemic metabolic processes that correlated with differences in mechanism of action between drugs, that is, direct tumor cell kill or initial vascular shutdown. **Conclusion:** Real-time follow-up of tumor response to PDT as monitored by dynamic ^{18}F-FDG PET has been shown to correlate with the mechanisms of action of photosensitizing drugs in vivo. This new imaging paradigm can be exploited to monitor a variety of transient cellular and molecular processes as they occur in vivo, enabling the mechanisms of action of therapeutic interventions to be scrutinized and their efficacy predicted in real time.

Key Words: small-animal PET; FDG; photodynamic therapy (PDT); photosensitizer; transient metabolic process; tumor

J Nucl Med 2006; 47:1119–1126

Photodynamic therapy (PDT) is a promising treatment for light-accessible tumors (*1*). This type of therapy combines tumor-localizing photosensitizers, visible light, and molecular oxygen to induce oxidative damage to the tumor tissue (*2*). Most clinical applications of PDT use porfimer sodium (Photofrin; Axcan Pharma PDT Inc.) (*3*), a mixture of hematoporphyrin derivatives, but second-generation photosensitizers such as the metallophthalocyanines (Pc) with better photochemical properties than porfimer sodium have been developed (*4*). Phthalocyanines form stable chelates with metal cations such as Zn^{2+} and Al^{3+}, and the addition of sulfonate groups at the periphery of the macro cycle gives water-soluble photosensitizers with well-documented potential for use in clinical PDT (*5*). The results of many studies of PDT in rodents have provided evidence for 2 types of response mechanisms that lead to tumor regression (*6*). PDT may cause direct tumor cell kill or activate endothelial cells to release vasoactive compounds that provoke vascular stasis followed by indirect damage to malignant cells. In addition to cell or vascular damage, release of vasoactive components may produce an inflammatory response into the tumor and surrounding tissues. The relative contribution of the 2 main pathways to overall tumor response depends on the distribution of the photosensitizer among cellular or vascular compartments, which in turn depends on the chemical nature of the photosensitizing drug (*7*). More hydrophobic or amphophilic photosensitizers such as disulfonated $ZnPcS_2$ are preferentially transported by lipoproteins, which are taken up directly by tumor cells, whereas hydrophilic photosensitizers such as tetrasulfonated $AlPcS_4$ are transported largely by albumin and deposited mainly in the vascular stroma of tumors (*8*). It follows that $ZnPcS_2$-PDT induces largely direct cell kill, whereas with $AlPcS_4$-PDT, the tumor vascular system is initially affected and indirect tumor cell death occurs afterward (*9,10*).

Small-animal PET is an excellent in vivo method to investigate various processes in molecular biology, oncology,

Received Sep. 2, 2005; revision accepted Dec. 1, 2005.

For correspondence or reprints contact: Roger Lecomte, PhD, Department of Nuclear Medicine and Radiobiology, Faculty of Medicine and Health Sciences, Université de Sherbrooke, 3001 12th Ave. N., CRC/CHUS #1864, Sherbrooke, QC, Canada, J1H 5N4.

E-mail: Roger.Lecomte@USherbrooke.ca

and neuroscience research (*11–14*). In oncologic PET studies, the most widely used radiopharmaceutical for the evaluation of tumor glucose metabolic rates is ^{18}F-FDG (*15,16*). ^{18}F-FDG PET appears also to be a promising method to study the effect of PDT in vivo, either to assess the efficacy of a photosensitizing drug or to determine its mechanism of action (*17,18*). Our previous study showed that the tissue uptake pattern of ^{18}F-FDG and the reduced metabolic activity of the treated tumor measured by PET at different times after PDT correlated with the mechanism of action of PDT through indirect vascular stasis or direct cell kill (*17*). We observed, in particular, that the effect of the PDT drug on the vascular system caused an early drop of ^{18}F-FDG uptake in the treated tumor, within less than 30 min after the end of the PDT light treatment. In contrast, the direct effect of the PDT drug on tumor cells appeared to be delayed by about 2 h after treatment.

Whereas these studies provided clear evidence of dissimilar modes of action for the 2 different PDT drugs, the simple measurement of ^{18}F-FDG tumor uptake at 2 time points gave little insight into the actual mechanisms of action leading to inactivation of the tumor cells. Further investigations of the tumor metabolism at specific intervals after illumination by the Patlak method confirmed these findings (*19*) but were of little help in unraveling the biologic processes that occur during and immediately after the light treatment and result in tumor cell obliteration. The reason they were of little help is due to 2 major problems with the conventional dynamic PET approach after a bolus injection of the radiotracer. First, the long uptake period of ^{18}F-FDG by tumors (>30 min) does not allow an instantaneous measurement of the metabolic state of tumor tissues but, rather, represents some average value over a specified interval. This is fine for a tumor (or any other tissue) in a steady state but is confounding for tissues undergoing rapid transient metabolic processes. The second related problem is that the effect of PDT treatment continues to evolve during the ^{18}F-FDG uptake period, hence preventing any instantaneous transient metabolic processes from being clearly differentiated.

This study explored the potential of using real-time dynamic ^{18}F-FDG PET with constant radiotracer infusion as a means to evaluate the role of the photosensitizer in the PDT tumor response mechanism. The photosensitizers selected for this study are known to induce tumor regression via different pathways, that is, via direct tumor cell kill and via indirect tumor cell kill for $ZnPcS_2$ photosensitizers and $AlPcS_4$ photosensitizers, respectively.

MATERIALS AND METHODS

Photosensitizers

Adjacently disulfonated $ZnPcS_2$ and tetrasulfonated $AlPcS_4$ (Fig. 1) were synthesized by a condensation method previously detailed (*20*). A few milligrams of Pc were dissolved in phosphate-buffered saline (PBS), 1 mmol/L, and sonicated for a few minutes. The solutions were filtered on Millex-GV, 0.22 μm (Millipore), under sterile conditions. The concentration of the dye solutions was determined by ultraviolet and visible absorption spectroscopy after dilution in dimethyl formamide ($\varepsilon = 2.5 \times 10^{-5}$ (mol/L)$^{-1}$cm^{-1} at $\lambda = 675$ nm). The working solutions were prepared by diluting the stock solutions in PBS such as to give final drug doses of 1 and 7.2 μmol/kg for $ZnPcS_2$ and $AlPcS_4$, respectively, in a total volume of 1 mL/100 g of body weight.

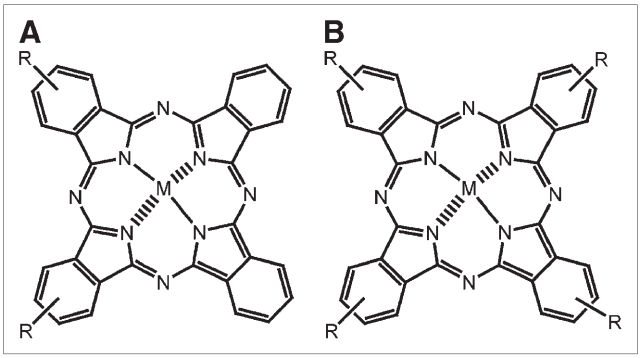

FIGURE 1. Chemical structure of $ZnPcS_2$ (A) and $AlPcS_4$ (B). M in A and B = zinc and aluminum, respectively; R = SO_3.

Animal Model

All experiments were performed on Fischer 344/CRBL female rats (150−160 g) (Charles River Breeding Laboratories) bearing two 13762 mammary adenocarcinoma tumors. The experiments followed a protocol approved by the Canadian Council on Animal Care and the in-house ethics committee. Animals were allowed free access to water and food throughout the experiments, except for the night preceding the ^{18}F-FDG PET study, when they were kept fasting.

Tumor Implantation

Mammary adenocarcinoma tumor cells (2.25×10^6 cells in 0.15 mL of PBS) were intradermally implanted in both axillary areas of each rat. The 2 tumors were allowed to grow 7 d before the PDT PET studies (tumor size: length [l] = 14.4−15.1 mm; width [w] = 9.8−11.9 mm; thickness [h] = 7.6−8.2 mm). Tumor volume was measured externally with an electronic caliper according to a hemiellipsoid model ($1/2\ [4\pi/3] \times [l/2] \times [w/2] \times h$). No tumor necrosis was evident at the time of treatment.

PDT

The day before the PDT PET study, the rats were given 1 μmol of $ZnPcS_2$ or 7.2 μmol of $AlPcS_4$ per kilogram of body weight through the tail vein (in 1 mL of PBS/100 g of body weight), representing the minimal dye dose required for total tumor regression after PDT. The PDT light treatment was applied 24 h after dye administration during the ^{18}F-FDG PET study. One tumor was illuminated with a 670-nm light beam delivered via a fiber optic by a diode laser (model BWF-670-300; B&W Tek, Inc.), and the other tumor was masked and served as a control. The light beam was spread uniformly over the whole tumor area and maintained for 2,000 s at a fluence rate of 200 mW/cm^2, to give a total fluence of 400 J/cm^2.

PET Studies

PET was performed with the Sherbrooke small-animal PET scanner (*21*). The scanner is made of 2 avalanche photodiode detector rings and produces 3 image planes (2 direct, 1 cross) over

a 1-cm axial field of view. The scanner has a flexible system of acquiring list-mode data that allows elaborate dynamic PET image series to be extracted as desired. The rats were anesthetized (2.5% isoflurane in medical O_2), and a butterfly cannula (Butterfly-25 Short; Venisystems) was placed in the tail vein. The position of the scanner bed was adjusted in order to place the tumors at the center of the axial field of view with the help of a laser pointer. Thirty minutes before the onset of illumination, a continuous infusion of ^{18}F-FDG (~250 MBq in 0.96 mL of PBS at 0.008 mL/min) was started while a 2-h dynamic PET image acquisition was launched. One tumor was illuminated for 2,000 s, and imaging was then continued for about another hour to complete the total 2-h scan sequence. The vital signs of the animals were monitored and recorded throughout the 2 h to ensure a stable physiologic status at all times. PET images consisting of 120 frames of 60 s each were sorted out from the list-mode data for each of the 3 planes and reconstructed by a maximum-likelihood expectation maximization algorithm implementing detector response (*22*). Four rats were scanned for each photosensitizer. Controls included scans of 2 rats that received photosensitizer but no light and scans of 2 rats that received light but no photosensitizer.

Image Analysis

Regions of interest were traced over the control and treated tumors on the last frame of the dynamic image series and applied to all preceding frames. Time–activity curves corrected for radionuclide decay were generated, and a mathematic model was used to fit 3 distinct parts of the curves corresponding to radiotracer uptake before, during, and after the illumination period. The following equations were used to fit the curves from the treated and untreated tumors:

$$f_1(t) = m_1 t - b_1(1 - e^{-m_1 t/b_1}) \quad 0 \le t \le T_i$$
$$f_2(t) = m_2 t - b_2 \quad T_i + \Delta 1 \le t \le T_f$$
$$f_3(t) = m_3 t - b_3 \quad T_f + \Delta 2 \le t \le 120\,\text{min},$$

where t is the time and m_1, m_2, and m_3 are the slope values representing tumor ^{18}F-FDG uptake rates before, during, and after PDT illumination, respectively. The b_i variables are fitting parameters that have no special meaning. Two additional parameters were introduced to describe the duration of the transient states that resulted from the intervention and were observable from the tumor ^{18}F-FDG uptake curves: response delay $\Delta 1$, which is the time lag after the start of illumination, T_i, until the ^{18}F-FDG uptake rate starts to drop, and recovery delay $\Delta 2$, which is the time lag after the end of illumination, T_f, until the ^{18}F-FDG uptake rate recovers. These 2 delay parameters were extracted from the intersections of the equations fitted to the 3 steady-state parts of the tumor ^{18}F-FDG uptake curves.

Statistical Analysis

The values reported represent the average ± SD over the number of subjects in each group. The significance of differences between mean values was determined by the Student *t* test.

RESULTS

The experimental protocol used for this investigation is illustrated in Figure 2. Changes in tumor ^{18}F-FDG uptake were visible on the PET scans (60 s each) obtained during the 2-h real-time ^{18}F-FDG PET sequence (Fig. 3). The accumulation of ^{18}F-FDG in treated tumor dropped significantly during the illumination period, followed by partial recovery on termination of the light treatment.

Differences in ^{18}F-FDG uptake between the 2 PDT protocols were more clearly visible from the ^{18}F-FDG time–activity curves taken over the untreated and light-treated tumors (Figs. 4A and 4B). Both $ZnPcS_2$-PDT and $AlPcS_4$-PDT induced a drop in the ^{18}F-FDG uptake rate followed by a partial recovery some time after the end of the illumination period, but with different response patterns. Both control scans, that is, administered photosensitizer without light treatment or light treatment without photosensitizer, showed a steady increase in ^{18}F-FDG uptake by both tumors (Figs. 4C and 4D). The differences in baseline ^{18}F-FDG uptake before PDT illumination resulted solely from the different tumor states at the time of the procedure.

Analysis of the ^{18}F-FDG time–activity curves, as depicted for $ZnPcS_2$-PDT in Figure 5, showed that the 3 distinctly different steady phases—m_1, m_2, and m_3—and 2 transient regions characterized by response delays—$\Delta 1$ and $\Delta 2$—properly describe the ^{18}F-FDG uptake rate. Combined, these parameters enabled clear discrimination between direct and indirect mechanisms of tumor cell kill but also provided some insight into the mechanisms of action of different drugs early during the photodynamic process.

The effect of the photosensitizer on PDT tumor response is summarized by the average ^{18}F-FDG uptake rates (Fig. 6) and response-recovery delays (Fig. 7) of 4 independent experiments. In the case of $ZnPcS_2$-PDT, which induces substantially direct tumor cell kill, the rate dropped dramatically (>90%) within 4 min after the start of the light treatment

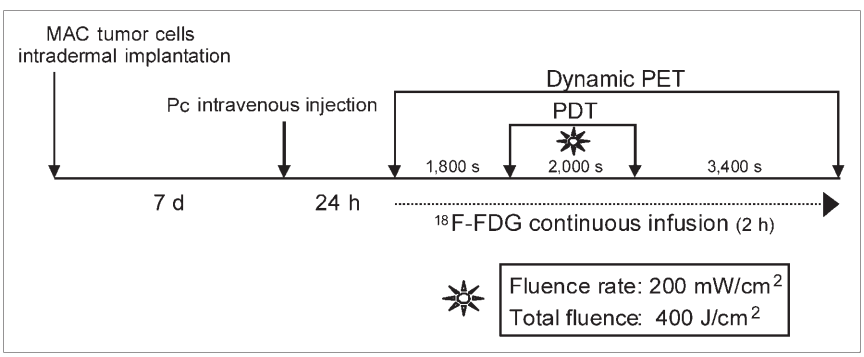

FIGURE 2. Schematic representation of steps of experimental PDT PET protocol.

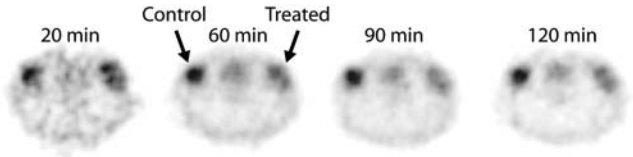

FIGURE 3. Selected ^{18}F-FDG PET image frames (1-min duration) taken at different times during $ZnPcS_2$-PDT treatment. Although ^{18}F-FDG uptake is comparable in the 2 tumors before PDT treatment (20 min), uptake is significantly reduced at end of light treatment (60 min) in treated tumor relative to control. Partial recovery of ^{18}F-FDG uptake is apparent after treatment (90 min) and even more so at end of imaging sequence (120 min).

while recovering to about 80% of the initial rate within 10 min after the end of the treatment, as is illustrated in Figure 6A for ^{18}F-FDG uptake rates and Figure 7 for response-recovery delays. The control tumor also showed a 50% drop in the ^{18}F-FDG uptake rate during PDT, followed by complete recovery after the treatment, suggesting a systemic response during the illumination phase (Fig. 6A). In the case of $AlPcS_4$-PDT, which acts largely via vascular stasis, this systemic component was small (<10% drop in ^{18}F-FDG uptake rate), although the ^{18}F-FDG uptake rate by the control tumor showed a slight but significant (~30%) increase after completion of the light treatment (Fig. 6B). The ^{18}F-FDG uptake rate in the illuminated tumor with $AlPcS_4$-PDT dropped by 70% (Fig. 6B) after a relatively long response lag of nearly 10 min (Fig. 7). Even more significant was the long lag of almost 25 min after $AlPcS_4$-PDT (Fig. 7) before the ^{18}F-FDG uptake rate recovered to about 60% of the initial rate (Fig. 6B).

DISCUSSION

Mechanisms of Action

PDT requires 3 components: a photosensitizer, molecular oxygen, and red light. Combined, they generate singlet

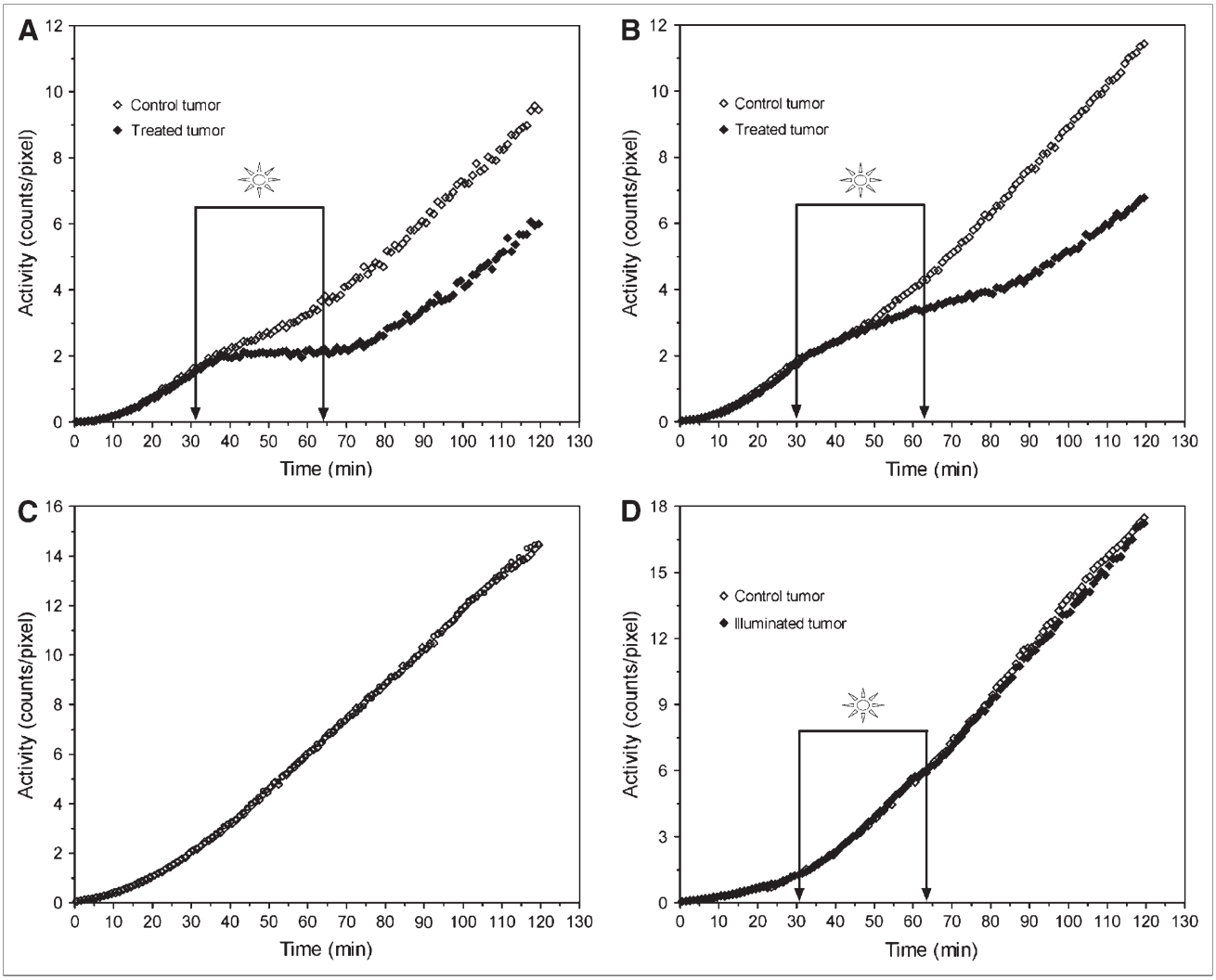

FIGURE 4. Typical ^{18}F-FDG tumor uptake curves during real-time ^{18}F-FDG PET study. Two tumors were implanted in each animal, but only one tumor received light treatment. ^{18}F-FDG uptake curves were generated for treated and untreated tumors during $ZnPcS_2$-PDT (A), during $AlPcS_4$-PDT (B), during control treatment with $ZnPcS_2$ without light (C), and during control treatment without photosensitizer but with light (D).

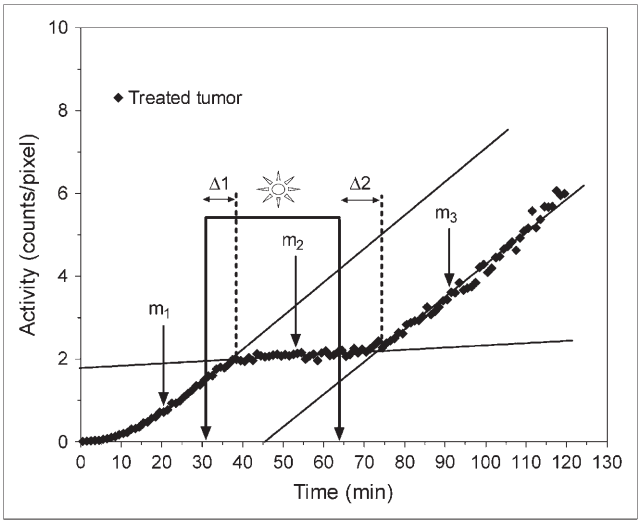

FIGURE 5. ^{18}F-FDG tumor uptake curve during $ZnPcS_2$-PDT treatment depicting the 3 distinct ^{18}F-FDG uptake phases and 5 parameters used to describe uptake slopes, response delay time (Δ1), and recovery delay time (Δ2).

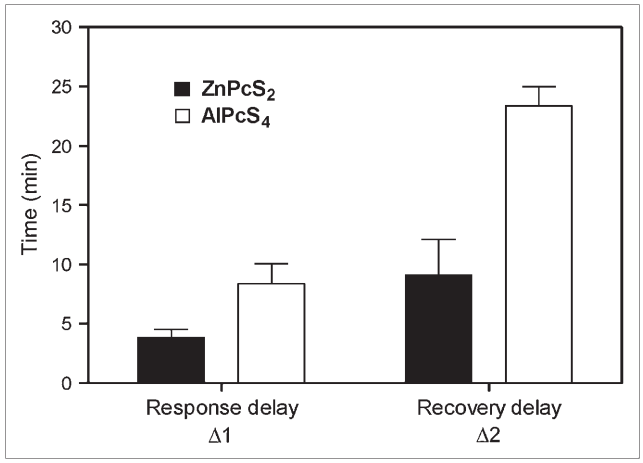

FIGURE 7. Histogram representing mean (±SD) response delay (Δ1) and recovery delay (Δ2), in minutes. Data were obtained from studies with $ZnPcS_2$-PDT (n = 4) and with $AlPcS_4$-PDT (n = 4).

oxygen, which is believed to be the principal cytotoxic entity, resulting in localized oxidative stress (*23*). Because of the high reactivity of singlet oxygen, this species exerts its detrimental action at the site of photosensitizer retention. Thus, the mechanism of action by which PDT induces tumor cell death depends largely on the localization of the photosensitizer during exposure to light. Chemical modifications that change the solubility of a photosensitizer without affecting its photochemical properties can significantly affect the outcome of PDT by modulating pharmacokinetics and tissue distribution. The photosensitizers selected for this study are known to target different tumor components. The amphophilic, disulfonated $ZnPcS_2$ has good cell membrane–penetrating properties and targets subcellular membrane structures. Furthermore, binding to lipoproteins favors retention by tumor tissue through interaction with low-density-lipoprotein receptors that are overexpressed at the membrane of most tumor cells (*24–26*). In contrast, the highly water-soluble, tetra-substituted $AlPcS_4$ is transported by serum albumin, resulting in accumulation within the interstitial space and vascular stroma of the tumor tissue (*27*). Thus, whereas $ZnPcS_2$ readily localizes in tumor cells after intravenous injection, $AlPcS_4$ remains in the tumor vascular compartment. The photosensitizer distribution pattern has obvious implications for the mechanisms by which PDT will induce tumor regression. PDT with $ZnPcS_2$ impairs mitochondrial and other intracellular membrane systems, resulting in direct tumor cell kill, whereas PDT with $AlPcS_4$ damages tumor blood vessels, interrupting the supply of oxygen and nutrients, resulting in indirect tumor cell death (*28,29*). In addition, varying the interval between drug administration and light exposure will affect the localization of a selected photosensitizer and, consequently, the way it will act (*30*). For example, PDT with the amphophilic $AlPcS_2$ resulted in severe vascular damage to a LOX tumor model when light was applied shortly after drug injection, whereas direct tumor cell damage was observed when the illumination was performed 48 h after drug administration (*31*). The PDT protocol and photosensitizers used for this ^{18}F-FDG PET study were selected such that $ZnPcS_2$-PDT induced mainly direct

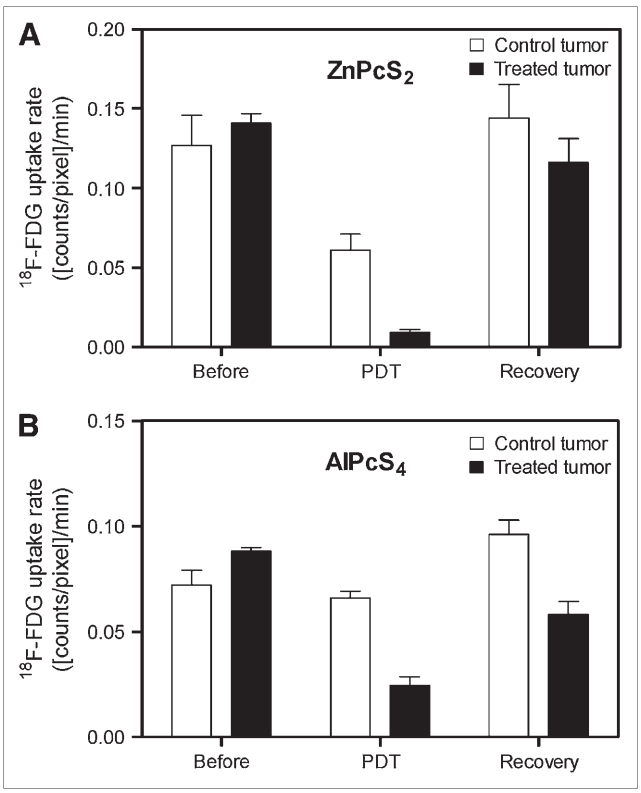

FIGURE 6. Histograms representing mean (±SD) tumor ^{18}F-FDG uptake rates (counts/pixel/min) before, during, and after illumination. Data were obtained from studies with $ZnPcS_2$-PDT (n = 4) (A) and with $AlPcS_4$-PDT (n = 4) (B).

tumor cell kill whereas $AlPcS_4$-PDT provoked vascular damage.

In our experiments, changes in the ^{18}F-FDG uptake profiles of treated tumors were more readily explained by the underlying mechanisms of action. In the case of $ZnPcS_2$-PDT, direct PDT-induced damage to tumor cell membranes might result in a loss of glucose transporter or hexokinase activity, either of which would rapidly reduce the rate of ^{18}F-FDG uptake by tumors. The ^{18}F-FDG uptake rate rapidly recovered to more than 80% of the initial rate, suggesting that most of the damage was reversible (Fig. 6A). However, other factors might have contributed to this resurgence. Apoptosis is well known to be a major response to the intracellular damage inflicted by PDT (*32*). The fact that the apoptotic pathway also requires energy (*33*) could explain, at least in part, the increase in ^{18}F-FDG uptake by the treated tumor. In addition, infiltration of inflammatory cells and the presence of residual viable tumor cells might also have contributed to maintaining the ^{18}F-FDG uptake rate (*34*).

In the case of $AlPcS_4$-PDT, damage to the vascular system was reflected in the delayed drop in the ^{18}F-FDG uptake rate and the long recovery period of more than 20 min after the illumination ended. The recovery delay was 3 times longer than that observed in the case of the direct cell kill mechanism (Fig. 7). Also, the recovered ^{18}F-FDG uptake rate remained substantially lower than the initial rate (Fig. 6B), suggesting that irreversible vascular damage limited blood flow and ^{18}F-FDG transport to the tumor tissue. Again, other factors, including inflammatory cell infiltration and reversible damage, might also have contributed to the increase in the ^{18}F-FDG uptake rate.

Other investigations using alternate, more specific radiotracers that are not subjected to secondary confounding effects such as inflammation or apoptosis would have to be considered to unravel the origin of the resurgence in ^{18}F-FDG tumor uptake after PDT. We are currently investigating the feasibility of using the perfusion tracers ^{13}N-ammonia and ^{64}Cu-labeled pyruvaldehyde bis(N^4-methylthiosemicarbazone) to measure tumor blood flow during and after PDT. Promising new tracers such as ^{18}F-fluorothymidine (*35*) or ^{18}F-fluoroethyltyrosine (*36*) could also be used with the same dynamic PET protocol as is used for ^{18}F-FDG to measure real-time variations in cell proliferation or protein synthesis during and after PDT. The observation period could likely be extended with little modification to the protocol to determine the duration and extent of transient metabolic processes after PDT.

Systemic Response

Even when shielded from light, the control tumor in the $ZnPcS_2$-PDT protocol showed reduced ^{18}F-FDG uptake during the illumination phase, suggesting a systemic response originating from the treated tumor (Fig. 6A). In the case of the $AlPcS_4$-PDT protocol, ^{18}F-FDG uptake by the control tumor was only slightly affected during the illumination phase (Fig. 6B). However, its uptake rate increased significantly ($P < 0.05$) after PDT, suggesting augmented metabolic activity. Hence, the control tumors in both cases showed variations in ^{18}F-FDG uptake resulting from the illumination phase, suggesting a systemic response originating from the treated tumors. Any uncorrelated effect of the photosensitizer or light treatment alone can be discarded, as confirmed by the control scans without light treatment and without photosensitizer (Figs. 4C and 4D). The systemic response likely results from the release of signaling factors at the site of the treated tumor. Damage to the vascular endothelium or platelets is well known to lead to production of various vasoactive compounds, including eicosanoids such as thromboxane, cytokines, clotting factors, and histamine. This in turn leads to increased vascular permeability to macromolecules, constriction of vessels, and eventually blood-flow stasis (*37,38*). Thus, although these vasoactive factors are released at the site of illumination, they may enter the blood circulation to act on remote blood vessels, including those of the control tumor, causing vasoconstriction and the observed drop in ^{18}F-FDG uptake by the distant tumor.

Although this series of events has been shown to occur with photosensitizers localizing in the vascular stroma of tumors, that is, those acting via an indirect mechanism, photosensitizers acting directly on tumor cells may have a similar effect. For instance, PDT of hamster ovary cells in vitro resulted in loss of cell integrity and the release of inflammatory and immune mediators, including eicosanoids and histamine (*39*). Therefore, both $AlPcS_4$-PDT– and $ZnPcS_2$-PDT–induced release of vasoactive molecules may explain, at least in part, the decrease in ^{18}F-FDG uptake by the illuminated tumor as well as by the control tumor. If, indeed, circulating vasoactive mediators affect the control tumor, this systemic effect will likely induce subtle changes in the vascular system of other organs. To this end, PET of possible alternative target organs, such as the heart, could be attempted to reveal the existence of a systemic vasoconstriction effect induced by localized photodynamic activity.

Pharmacokinetic Modeling

The aim of this study was to demonstrate the feasibility of real-time imaging of transient metabolic processes during PDT. With such an aim, this pilot study did not attempt quantitative modeling of ^{18}F-FDG uptake. The continuous-infusion protocol was designed, in the first place, to circumvent the limitations of multiple bolus injections of ^{18}F-FDG, as were previously used to follow PDT kinetics (*17*). Deriving quantitative values from the observed changes in perfusion and metabolic activities will require the design and validation of a proper kinetic model, which will be addressed in future studies.

Future Perspectives

Even though these real-time ^{18}F-FDG PET studies leave many unanswered questions on complex PDT tumor

response mechanisms, the dissimilar transient metabolic processes revealed by changes in ^{18}F-FDG uptake rates and response delays are striking evidence of different modes of action. The dramatic differences in ^{18}F-FDG uptake profiles provide a rapid, real-time way to distinguish between direct and indirect mechanisms of tumor cell destruction and to assist in characterizing the photosensitizer and the PDT protocol. This is in sharp contrast to conventional, visual tumor response follow-up procedures that usually require many weeks of observation (*40*). Obviously, ^{18}F-FDG PET can also be used to follow tumor regression after PDT at later intervals (*17*). However, the clear advantage of continuous ^{18}F-FDG infusion and dynamic PET over other methods of assessing tumor response lies in its potential to reveal tumor response in real time, enabling the sequence of subtle transient metabolic processes within tumor tissues to be observed over time. In addition to identifying differences in mechanisms of action between various drugs, this technique allows for the rapid assessment of PDT protocols in order to optimize drug/light doses and their timing. In progress in our laboratory are further studies to expand real-time PET monitoring of tumor response to PDT by including radiotracers for blood flow, cell proliferation, hypoxia, and apoptosis. The same method could be considered to investigate the early response of tumors to other therapeutic approaches, such as chemotherapy or radiotherapy.

CONCLUSION

We have demonstrated the feasibility of using continuous ^{18}F-FDG infusion and dynamic PET to study tumor metabolic response in real time during PDT in a small-animal model. This use proved particularly applicable for investigating tumoral and systemic transient metabolic changes resulting from PDT treatment and for characterizing the mechanisms of action of different photosensitizing drugs. Such dynamic small-animal PET can also be used as a rapid screening procedure for selecting new drugs and for optimizing treatment protocols. Because tumor response to PDT involves both a metabolic and a vasorestrictive component, we are currently expanding the procedure by including a blood-flow PET tracer in our PDT PET studies. The concept that has been demonstrated here—dynamic PET combined with a constant radiotracer infusion—can be applied to the real-time monitoring of other transient cellular and molecular processes, such as cell proliferation, protein synthesis, hypoxia, and apoptosis during and immediately after therapeutic intervention.

ACKNOWLEDGMENTS

This work was supported by the Canadian Institutes of Health Research (CIHR grants MOP-44065 and MOP-15348). The authors would like to acknowledge the contribution of David Lapointe, who originally suggested the continuous infusion method used in this work to monitor tumor metabolic response in real time during PDT.

REFERENCES

1. Dougherty TJ. Photosensitizers: therapy and detection of malignant tumors. *Photochem Photobiol.* 1987;45:879–889.
2. Henderson BW, Dougherty TJ. How does photodynamic therapy work? *Photochem Photobiol.* 1992;55:145–157.
3. Dougherty TJ, Marcus SL. Photodynamic therapy. *Eur J Cancer.* 1992;28A: 1734–1742.
4. Sharman WM, Allen CM, van Lier JE. Photodynamic therapeutics: basic principles and clinical applications. *Drug Discov Today.* 1999;4: 507–517.
5. Allen CM, Sharman WM, van Lier JE. Current status of phthalocyanines in the photodynamic therapy of cancer. *J Porph Phthal.* 2001;5:161–169.
6. Oleinick NL, Evans HH. The photobiology of photodynamic therapy: cellular targets and mechanisms. *Radiat Res.* 1998;150(suppl):S146–S156.
7. Krammer B. Vascular effects of photodynamic therapy. *Anticancer Res.* 2001; 21:4271–4277.
8. Jori G. In vivo transport and pharmacokinetic behavior of tumour photosensitizers. *Ciba Found Symp.* 1989;146:78–86.
9. Chan WS, Brasseur N, La Madeleine C, Ouellet R, van Lier JE. Efficacy and mechanism of aluminium phthalocyanine and its sulphonated derivatives mediated photodynamic therapy on murine tumours. *Eur J Cancer.* 1997;33: 1855–1859.
10. Chan WS, Brasseur N, La Madeleine C, van Lier JE. Evidence for different mechanisms of EMT-6 tumor necrosis by photodynamic therapy with disulfonated aluminum phthalocyanine or Photofrin: tumor cell survival and blood flow. *Anticancer Res.* 1996;16:1887–1892.
11. Cherry SR, Gambhir SS. Use of positron emission tomography in animal research. *ILAR J.* 2001;42:219–232.
12. Herschman HR. Micro-PET imaging and small animal models of disease. *Curr Opin Immunol.* 2003;15:378–384.
13. Myers R. The biological application of small animal PET imaging. *Nucl Med Biol.* 2001;28:585–593.
14. West CM, Jones T, Price P. The potential of positron-emission tomography to study anticancer-drug resistance. *Nat Rev Cancer.* 2004;4:457–469.
15. Chaiken L, Rege S, Hoh C, et al. Positron emission tomography with fluorodeoxyglucose to evaluate tumor response and control after radiation-therapy. *Int J Radiat Oncol Biol Phys.* 1993;27:455–464.
16. Tatsumi M, Nakamoto Y, Traughber B, Marshall LT, Geschwind JFH, Wahl RL. Initial experience in small animal tumor imaging with a clinical positron emission tomography/computed tomography scanner using 2-[F-18]fluoro-2-deoxy-D-glucose. *Cancer Res.* 2003;63:6252–6257.
17. Lapointe D, Brasseur N, Cadorette J, et al. High-resolution PET imaging for in vivo monitoring of tumor response after photodynamic therapy in mice. *J Nucl Med.* 1999;40:876–882.
18. Moore JV, Waller ML, Zhao S, et al. Feasibility of imaging photodynamic injury to tumours by high-resolution positron emission tomography. *Eur J Nucl Med.* 1998;25:1248–1254.
19. Bentourkia M, Bérard V, Cadorette J, van Lier JE, Lecomte R. Assessment of tumor photodynamic therapy in the rat using small animal positron emission tomography [abstract]. *Mol Imaging Biol.* 2004;6:92.
20. Ali H, Langlois R, Wagner JR, Brasseur N, Paquette B, van Lier JE. Biological activities of phthalocyanines.10. Syntheses and analyses of sulfonated phthalocyanines. *Photochem Photobiol.* 1988;47:713–717.
21. Lecomte R, Cadorette J, Rodrigue S, et al. Initial results from the Sherbrooke avalanche photodiode positron tomograph. *IEEE Trans Nucl Sci.* 1996;43: 1952–1957.
22. Selivanov VV, Picard Y, Cadorette J, Rodrigue S, Lecomte R. Detector response models for statistical iterative image reconstruction in high resolution PET. *IEEE Trans Nucl Sci.* 2000;47:1168–1175.
23. Sharman WM, Allen CM, van Lier JE. Role of activated oxygen species in photodynamic therapy. *Methods Enzymol.* 2000;319:376–400.
24. Gèze M, Morlière P, Mazière JC, Smith KM, Santus R. Lysosomes, a key target of hydrophobic photosensitizers proposed for photochemotherapeutic applications. *J Photochem Photobiol B.* 1993;20:23–35.
25. Jori G, Beltramini M, Reddi E, et al. Evidence for a major role of plasma lipoproteins as hematoporphyrin carriers in vivo. *Cancer Lett.* 1984;24: 291–297.
26. Mazière JC, Morlière P, Santus R. The role of the low density lipoprotein receptor pathway in the delivery of lipophilic photosensitizers in the photodynamic therapy of tumours. *J Photochem Photobiol B.* 1991;8:351–360.
27. Kessel D, Thompson P, Saatio K, Nantwi KD. Tumor-localization and photosensitization by sulfonated derivatives of tetraphenylporphine. *Photochem Photobiol.* 1987;45:787–790.

28. Milanesi C, Zhou C, Biolo R, Jori G. Zn(II)-phthalocyanine as a photodynamic agent for tumours. II. Studies on the mechanism of photosensitised tumour necrosis. *Br J Cancer.* 1990;61:846–850.
29. van Lier JE, Spikes JD. The chemistry, photophysics and photosensitizing properties of phthalocyanines. *Ciba Found Symp.* 1989;146:17–32.
30. Peng Q, Moan J, Nesland JM. Correlation of subcellular and intratumoral photosensitizer localization with ultrastructural features after photodynamic therapy. *Ultrastruct Pathol.* 1996;20:109–129.
31. Peng Q, Moan J, Nesland JM, Rimington C. Aluminum phthalocyanines with asymmetrical lower sulfonation and with symmetrical higher sulfonation: a comparison of localizing and photosensitizing mechanism in human tumor LOX xenografts. *Int J Cancer.* 1990;46:719–726.
32. Oleinick NL, Morris RL, Belichenko I. The role of apoptosis in response to photodynamic therapy: what, where, why, and how. *Photochem Photobiol Sci.* 2002;1:1–21.
33. Oberdanner CB, Kiesslich T, Krammer B, Plaetzer K. Glucose is required to maintain high ATP-levels for the energy-utilizing steps during PDT-induced apoptosis. *Photochem Photobiol.* 2002;76:695–703.
34. Findlay M, Young H, Cunningham D, et al. Noninvasive monitoring of tumor metabolism using fluorodeoxyglucose and positron emission tomography in colorectal cancer liver metastases: correlation with tumor response to fluorouracil. *J Clin Oncol.* 1996;14:700–708.
35. Sugiyama M, Sakahara H, Sato K, et al. Evaluation of 3′-deoxy-3′-^{18}F-fluorothymidine for monitoring tumor response to radiotherapy and photodynamic therapy in mice. *J Nucl Med.* 2004;45:1754–1758.
36. Pauleit D, Stoffels G, Schaden W, et al. PET with O-(2-^{18}F-fluoroethyl)-L-tyrosine in peripheral tumors: first clinical results. *J Nucl Med.* 2005;46:411–416.
37. Ben-Hur E, Heldman E, Crane SW, Rosenthal I. Release of clotting factors from photosensitized endothelial cells: a possible trigger for blood vessel occlusion by photodynamic therapy. *FEBS Lett.* 1988;236:105–108.
38. Fingar VH. Vascular effects of photodynamic therapy. *J Clin Laser Med Surg.* 1996;14:323–328.
39. Bellnier DA, Dougherty TJ. Membrane lysis in Chinese hamster ovary cells treated with hematoporphyrin derivative plus light. *Photochem Photobiol.* 1982;36:43–47.
40. Margaron P, Madarnas P, Quellet R, van Lier JE. Biological activities of phthalocyanines. XVII histopathologic evidence for different mechanisms of EMT-6 tumor necrosis induced by photodynamic therapy with disulfonated aluminum phthalocyanine or Photofrin. *Anticancer Res.* 1996;16:613–620.